energies

MDPI

Article

Assessing the Impact of DFIG Synthetic Inertia Provision on Power System Small-Signal Stability

Edgar Lucas *, David Campos-Gaona and Olimpo Anaya-Lara

Department of Electronic and Electrical Engineering, University of Strathclyde, Glasgow G1 1XQ, UK; d.campos-gaona@strath.ac.uk (D.C.-G.); olimpo.anaya-lara@strath.ac.uk (O.A.-L.)

* Correspondence: edgar.lucas@strath.ac.uk

Received: 14 August 2019; Accepted: 4 September 2019; Published: 6 September 2019

Abstract: Synthetic inertia provision through the control of doubly-fed induction generator (DFIG) wind turbines is an effective means of providing frequency support to the wider electrical network. There are numerous control topologies to achieve this, many of which work by making modifications to the DFIG power controller and introducing additional loops to relate active power to electrical frequency. How these many controller designs compare to one-another in terms of their contribution to frequency response is a much studied topic, but perhaps less studied is their effect on the small-signal stability of the system. The concept of small-signal stability in the context of a power system is the ability to maintain synchronism when subjected to small disturbances, such as those associated with a change in load or a loss of generation. Amendments made to the control system of a large-scale wind farm will inevitably have an effect on the system as a whole, and by making a DFIG wind turbine behave more like a synchronous generator, which synthetic inertia provision does, may incur consequences relating to electromechanical oscillations between generating units. This work compares the implications of two prominent synthetic inertia controllers of varying complexity and their effect on small-signal stability. Eigenvalue analysis is conducted to highlight the key information relating to electromechanical modes between generators for the two control strategies, with a focus on how these affect the damping ratios. It is shown that as the synthetic inertia controller becomes both more complex and more effective, the damping ratio of the electromechanical modes is reduced, signifying a decreased system stability.

Keywords: synthetic inertia; DFIG; small-signal stability

1. Introduction

Modern power systems are facing unprecedented levels of renewable energy penetration motivated by government targets and potential reductions in cost per MWh. The introduction of large scale wind power generation may lead to the decommissioning of conventional synchronous generators which will have a negative impact on the stability of the system of a whole. Without the large rotating masses and the associated inertia that these synchronous generators provide, the frequency of the system will become more sensitive to disturbances. Additionally, type-3 and type-4 variable speed wind turbines which are the most common topologies in new developments [1] are either partially or fully decoupled from the grid through power electronic converters, meaning that their inertia contributions cannot be 'seen' by the wider network. As the penetration of low inertia wind energy increases, the effect on power system stability becomes an important issue which needs to be analysed [2].

The concept of synthetic inertia is nothing new. Unlike a synchronous generator, the kinetic energy stored in the wind turbine blades cannot be readily accessed and can only be released through control action. The term synthetic comes from the fact that there is no instantaneous response to a drop

in frequency in the wider network and all action is achieved through the power electronic converter. The share of wind power is now so large that system operators are revising their grid codes such that wind farms require frequency control capabilities in specific conditions [3].

This paper looks to gain insight into how different synthetic inertia control strategies compare to each other in the context of small-signal stability by analysing the oscillatory electromechanical modes between synchronous generators. Low frequency oscillation of local modes between nearby generators and inter-area modes between generators in different areas can have detrimental effects on transmission capacity and stability of the system as a whole [4]. It is hypothesised that, although synthetic inertia control strategies provide the system with some much needed frequency support, the different methods of achieving this may have unintended downsides in reducing the damping ratio of the system and driving the network into the realms of instability.

1.1. Synthetic Inertia

This paper will focus on two methods of synthetic inertia provision, both of which work by providing an artificially manipulated set-point to the active power controller. The effect of this new set-point is to release a portion of the kinetic energy stored in the rotor and provide active power at the expense of a reduction in rotational speed. Clearly, this method cannot be sustained indefinitely due to the finite quantity of kinetic energy available, but to satisfy existing and proposed grid codes, only a small percentage of rated power needs to be provided for a limited time, typically below ten percent of the rated capacity [5–7]. For the purposes of this work, this value is exaggerated for demonstration purposes up to a maximum of 20% of the rated wind farm capacity. Whilst not impossible, this approach is unrealistic in a real-world environment but will be useful in demonstrating the core concepts.

The first method of synthetic inertia control, shown in Figure 1a, is a one-loop design based on the deviation of the system frequency from the nominal value [8,9]. This scheme is termed droop control and regulates the active power output from a wind turbine proportional to the change in frequency. There is a linear relationship between active power and frequency, and this control scheme adjusts the power set-point according to the linear characteristic in (1).

$$\Delta P = -\frac{f_{meas} - f_{nom}}{R} \tag{1}$$

where f_{meas} is the new frequency, f_{nom} is the initial operating point and R is the droop constant.

The second control strategy to be considered is the two-loop design shown in Figure 1b. This scheme provides a modified power reference which is proportional to frequency deviation and lasts until nominal frequency is restored.The first loop acts when the rate of change of frequency is high, while the Δf loop has a strong effect when the system frequency differs greatly from the nominal value. The values of K1 and K2 are selected based on the desired level of synthetic inertia provided by the DFIG. The effects of changing K1 and K2 are discussed in more detail in [10].

1.2. Modelling

The model used for simulation is based on a two-area network featuring three synchronous machines and a wind farm. In the absence of an infinite bus, a load must be connected to the central bus to balance the power flow and maintain synchronism. These components are connected to each other via a set of network equations which define the admittance matrix of the system. A schematic layout of the system is shown in Figure 2 which identifies the two areas. Tables A1 and A2 in Appendix A give the parameters of the machines.

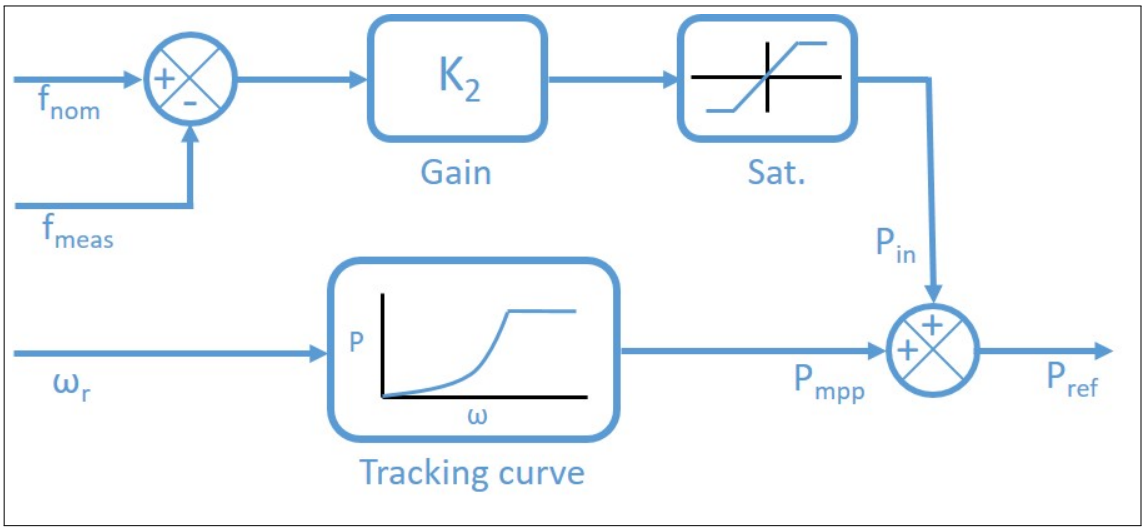

(**a**)

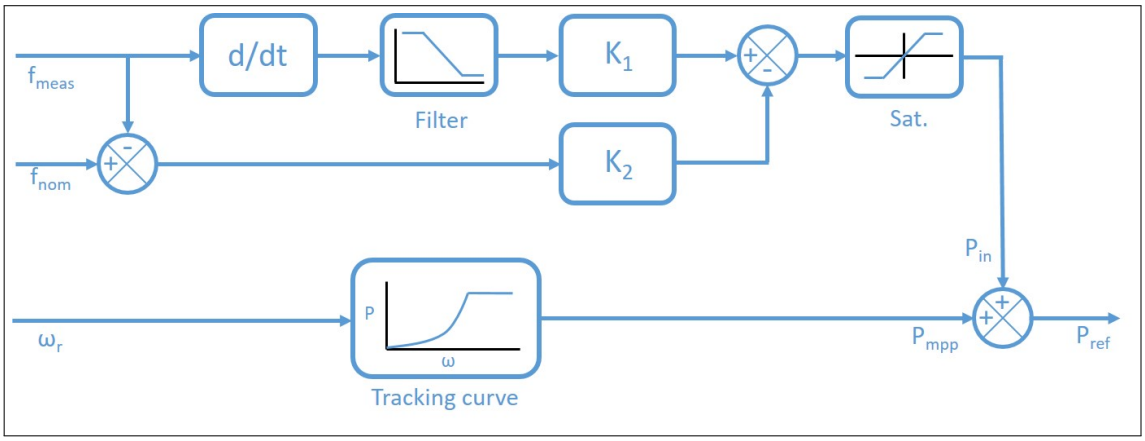

(**b**)

Figure 1. (**a**) One-loop synthetic inertia control strategy, (**b**) Two-loop synthetic inertia control strategy.

The machines are sized such that generator 1 is five times larger in capacity than generators two and three, rated at 1000, 200 and 200 MW, respectively. Generator 1 is fitted with a simple governor to regulate rotor speed via an applied torque and to fix the network frequency at the nominal value. Generator 1 is therefore termed the balancing machine. The DFIG represents an entire wind farm of identical individual turbines with an aggregated power of 100 MW.

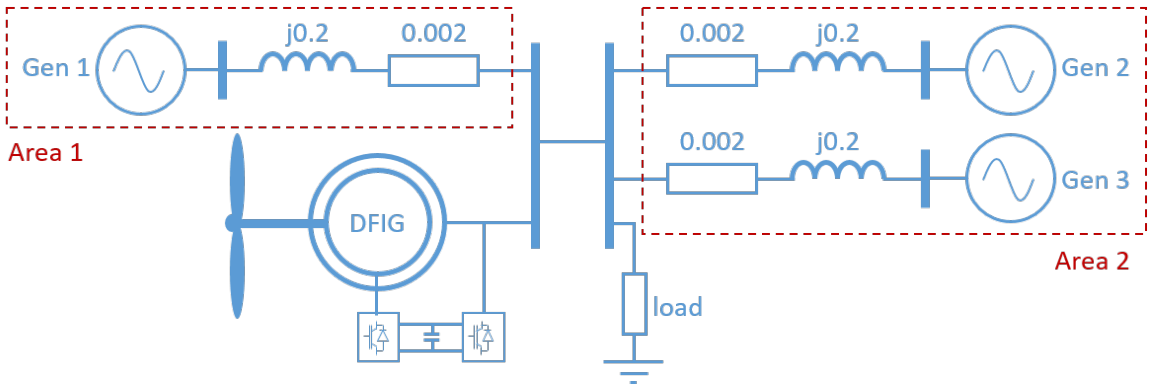

Figure 2. Two-area network used in simulation.

The network model uses the transient model of a synchronous generator in the dq-reference frame in which the stator dynamics are neglected. The resulting set of differential equations are fourth order: two differential equations describe the rotor dynamics and the remaining two are used to describe the rotor speed and angle [11]. The DFIG is modelled as a fifth order system in the dq-reference frame. Since every element of the network is modelled in dq, the effects of the PLL can be neglected. This is because operating in the dq reference frame is equivalent to having an ideal PLL. The full set of network equations and parameters are provided in Appendix A.

Control of the DFIG is achieved by directly manipulating the rotor voltages in the dq-frame, negating the need to model the back-to-back converter. This method is based on the internal mode control presented in [12]. Since this paper is only focused on the active power controller which operates entirely in the d-axis, further simplifications can be made by omitting any q-axis components relating to reactive power.

2. Linearisation

Small-signal stability defined in the context of a power system is the ability to maintain synchronism when subjected to small perturbations [13]. The term 'small' implies that the equations describing the response may be linearised for analysis, which is the focus of this section.

The power system under consideration is given by a set of n linearly independent state variables of the form in (2), where x_i are the state variables, u_i are the inputs to the model and t is time. The complete set of differential equations is provided in Appendix A. The state variables are a combination of physical quantities such as angle and speed, and other more abstract mathematical variables associated with the differential equations that describe the dynamics of the system [13].

$$\dot{x} = f_i(x_1, ..., x_n; u_1, ..., u_m; t) \quad i = 1, \dots, n \tag{2}$$

To begin the linearisation process, a set of equilibrium points must first be defined. These are the points where all of the derivative terms are simultaneously zero, implying that the system is at rest and all of the variables are constant with respect to time. Mathematically, this implies that $f(x_0) = 0$, with x_0 being an operating point. Due to the complexity of a multi-machine system, the equilibrium points of the model considered in this paper are determined from simulation. After a sufficiently long settling time, a snapshot is taken of the state variables when they are in steady-state and saved to file. This is done multiple times for different operating conditions and control strategies until a complete set of equilibrium points exist for all scenarios. The system state equations are then obtained by linearisation at an equilibrium point:

$$\begin{bmatrix} \Delta\dot{x}_{DFIG} \\ \Delta\dot{x}_{GOV} \\ \Delta\dot{x}_{SG_n} \end{bmatrix} = \mathbf{A} \begin{bmatrix} \Delta x_{DFIG} \\ \Delta x_{GOV} \\ \Delta x_{SG_n} \end{bmatrix} \tag{3}$$

where

$$x_{DFIG} = \begin{bmatrix} \omega_r & K_{iP} & \lambda_{ds} & \lambda_{qs} & \lambda_{dr} & \lambda_{qr} \end{bmatrix}^T \tag{4}$$

$$x_{GOV} = \begin{bmatrix} T_1 & T_2 & T_3 \end{bmatrix}^T \tag{5}$$

$$x_{SG_n} = \begin{bmatrix} \delta_n & \omega_n & E'_{d_n} & E'_{q_n} \end{bmatrix}^T \quad \text{for} \quad n = 1, 2, 3 \tag{6}$$

Here, ω_r is rotor speed of the doubly-fed induction generator, K_{iP} comes from the integral term in the power controller, λ are the fluxes, T_n are from the transfer functions of the governor, δ and ω are the angle and speed of the synchronous generators respectively and E'_{dq} are the two-axis transient emfs of the synchronous generators. For n = 3 generators, these states form a 21-order system.

Small-signal stability analysis is concerned with the eigenproperties of the Jacobian matrix **A**, which is of the form in (7). The entries in **A** give the coupling relationships between each of the dynamic processes [14]. The eigenvalues of **A** are of the form in (8).

$$\mathbf{A} = \begin{bmatrix} \frac{\partial f_1}{\partial x_1} & \cdots & \frac{\partial f_1}{\partial x_n} \\ \cdots & \cdots & \cdots \\ \frac{\partial f_n}{\partial x_1} & \cdots & \frac{\partial f_n}{\partial x_n} \end{bmatrix} \tag{7}$$

$$\lambda_i = \sigma_i \pm j\omega_i \quad \text{for} \quad i = 1, ..., n \tag{8}$$

For a complex pair of eigenvalues, the real component gives the damping and the imaginary component gives the frequency of oscillation. The frequency of oscillation is given by (9) and the damping ratio is given by (10). The damping ratio is of particular importance as this determines the rate of decay of the oscillations. A high damping ratio implies that any oscillations away from the static equilibrium will decay quickly, whereas a low damping ratio implies the opposite. A high value of ζ is desirable in the context of small-signal stability. It can be seen from Equation (10) that the value of ζ is largely dependant on the real component of a particular eigenvalue, such that a more-negative real component implies a higher damping ratio. This is analogous to the position of poles in control theory, where the system is stable if the poles are in the left hand plane, and a more negative real component results in a faster response. Note that it is also a necessary condition for stability that all eigenvalues have a negative real part.

$$f = \frac{\omega}{2\pi} \qquad (Hz) \tag{9}$$

$$\zeta = -\frac{\sigma}{\sqrt{\sigma^2 + \omega^2}} \tag{10}$$

There is no one-to-one relationship between any single eigenvalue and a particular state because they each belong to the system as a whole. It is therefore necessary to define the participation matrix **P** which provides a numerical score of a particular eigenvalue against a specific state. The participation matrix is generated from the matrices of right and left eigenvalues, Φ and Ψ respectively. Note that it is standard practice to normalise these matrices such that $\Psi\Phi = \mathbf{I}$.

$$\Phi = \begin{bmatrix} \phi_1 & \phi_2 & \cdots & \phi_n \end{bmatrix} \tag{11}$$

$$\Psi = \begin{bmatrix} \psi_1^T & \psi_2^T & \cdots & \psi_n^T \end{bmatrix}^T \tag{12}$$

where the right and left eigenvectors are given by Equations (13) and (14) respectively.

$$\mathbf{A}\phi_i = \lambda\phi_i = 0 \tag{13}$$

$$\psi_i\mathbf{A} = \lambda\psi_i = 0 \tag{14}$$

$$\phi_i = \begin{bmatrix} \phi_{1i} \\ \phi_{2i} \\ \cdots \\ \phi_{ni} \end{bmatrix} \quad ; \quad \psi_i = \begin{bmatrix} \psi_{1i} & \psi_{2i} & \cdots & \psi_{ni} \end{bmatrix} \tag{15}$$

The modal matrices Φ and Ψ are then used to form the participation matrix **P**, the entries of which will be used to determine the dominant eigenvalues for each state.

$$\mathbf{P} = \begin{bmatrix} p_1 & p_2 & \dots & p_n \end{bmatrix}$$
$$\text{where} \quad p_i = \begin{bmatrix} \phi_{1i}\psi_{i1} \\ \phi_{2i}\psi_{i2} \\ \dots \\ \phi_{ni}\psi_{in} \end{bmatrix} \tag{16}$$

$\phi_{ki} = k$th row, ith column of modal matrix Φ.
$\psi_{ik} = i$th row, kth column of modal matrix Ψ.

3. Results

The simulation will be run under three conditions in three different scenarios: no inertia control; one-loop control from Figure 1a and two-loop control from Figure 1b, for the three network scenarios defined below. The eigenproperties of the resulting state matrix will then be analysed to infer the behaviour of each control strategy in the wider context of the network.

1. Base case—system is operating normally;
2. Heavy load—the governor fitted to generator 1 is limited such that it can no longer provide additional power. The grid is now at full capacity and any imbalance between generation and load will be strongly reflected in the frequency characteristic;
3. Weak interconnection—the tie-line connecting generator 1 to the rest of the system is reduced in strength to represent a longer transmission line and a weaker grid.

3.1. Scenario 1—Base Case

For the base case of the model without any synthetic inertia control, the eigenvalues of **A** are given in Table 1, which shows the real and imaginary components, the frequency and damping ratio of each oscillatory mode and the associated dominant states as determined from the participation matrix.

From Table 1 it can be seen that there are several eigenvalues with rotor speed and angle as the dominant states. The terms $G()$ are used to specify the generators involved in each mode such that $G(1,2,3)$ affects all three generators from both areas, whereas $G(2,3)$ only applies to generators 2 and 3 which are confined to the same area. This demonstrates the concept of inter-area and local-area modes.

Since the mechanical dynamics of a DFIG are decoupled from the electric grid, they therefore do not participate in the modes of oscillation and instead interact either by displacing synchronous generators, or by interaction of the controllers with the damping torque of large generators [15]. This absence of coupling between the DFIG wind turbine and the synchronous generators is shown in Table 1. In the absence of synthetic inertia control the terms in matrix **A** which couple the DFIG to the synchronous generators are zero, meaning that the state variables of a wind turbine do not contribute to the electromechanical oscillations between synchronous generators. When the DFIG is made to behave more like a synchronous machine through synthetic inertia provision, a coupling is introduced such that the DFIG contributes to these oscillations [16,17]. However, this effect is strongly tied to the dynamics of the PLL and since this paper uses a purely dq-reference frame, the coupling is not seen even when synthetic inertia control is introduced [14].

In scenario 1, the system appears as in Figure 2. The simulation is initialised for each of the three control strategies using their respective equilibrium points for linearisation which results in a state-space model. The time-domain response of the three control designs can be seen in Figure 3, which shows an impulse being sent to the mechanical torque of generator 3 and the corresponding effect this has on the rotor speed and hence electrical frequency. One-loop control shows improved

recovery to a frequency disturbance as compared to no-control, while the two-loop improves on this with an even more reduced frequency nadir.

Table 1. Eigenvalues of state matrix—base case.

Eigenvalue	Real	Imaginary	Frequency	Damping	Dominant States
$\lambda_{1,2}$	−0.399	±368.00	58.569	0.001	λ_{ds},λ_{qs}
$\lambda_{3,4}$	−4.116	±80.19	12.763	0.051	λ_{dr}
$\lambda_{5,6}$	−2.524	±17.42	2.772	0.143	$\Delta\delta$, $\Delta\omega$ G(2,3)
$\lambda_{7,8}$	−2.315	±15.06	2.397	0.152	$\Delta\delta$, $\Delta\omega$ G(1,2,3)
$\lambda_{9,10}$	−4.326	±7.62	1.212	0.494	λ_{qr}
λ_{11}	−3.566	-	-	-	E'_d G(1,2,3)
λ_{12}	−3.351	-	-	-	E'_d G(2,3)
$\lambda_{13,14}$	−0.156	±2.31	0.368	0.067	T_1, $\Delta\delta$, $\Delta\omega$ G(1)
λ_{15}	−1.962	-	-	-	E'_d G(1,2,3)
λ_{16}	−0.376	-	-	-	E'_q G(2,3)
λ_{17}	−0.345	-	-	-	E'_q G(1,2,3)
λ_{18}	−0.157	-	-	-	E'_q G(1,2,3)
λ_{19}	−0.100	-	-	-	T_2
λ_{20}	−0.040	-	-	-	T_3
λ_{21}	0.000	-	-	-	Redundant

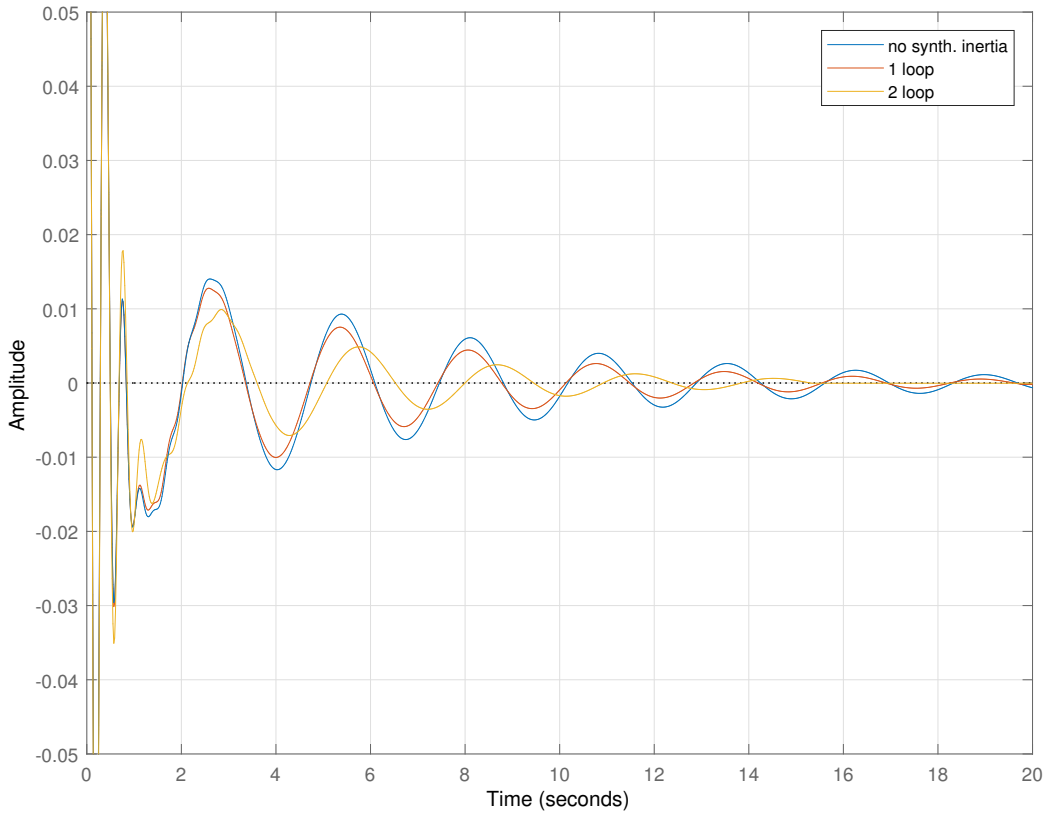

Figure 3. Impulse response of electrical frequency to a change in mechanical torque. Graph shows the deviation from the steady-state value.

It can be seen from Table 1 that the system is stable, characterised by the negative real parts of each eigenvalue. There are two rotor angle modes of oscillation: the inter-area mode of G(1,2,3) and the local-area mode between G(2,3) identified from the table as $\lambda_{5,6}$ and $\lambda_{7,8}$. The mode shapes are plotted in Figure 4a which shows the swinging of generator 1 with generators 2 and 3, and Figure 4b which shows the swinging of generator 2 with generator 3.

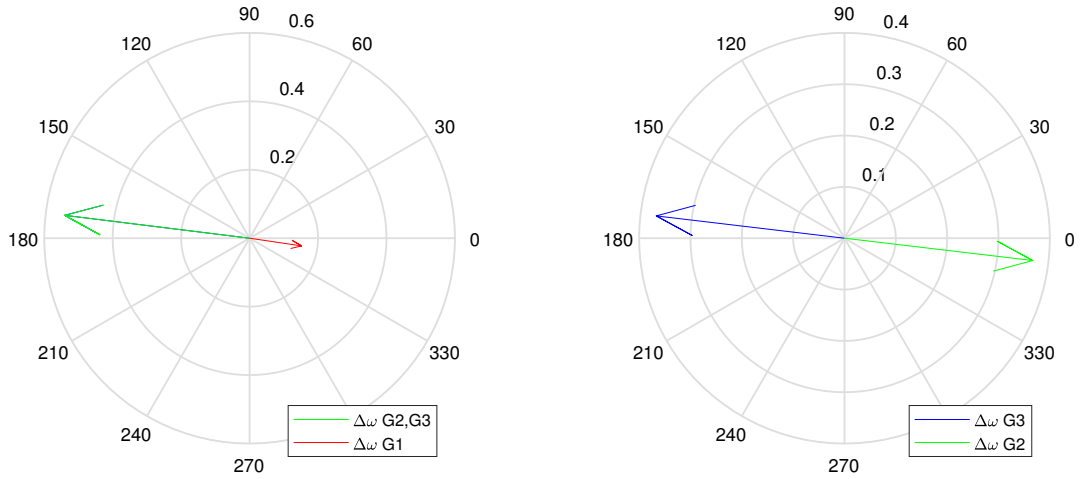

(**a**) Inter-area mode (**b**) Local-area mode

Figure 4. (**a**) Inter-area mode showing the swing of generator 1 with generators 2 and 3. (**b**) Local area mode showing the swing of generator 2 with generator 3.

Figure 5 is a pole plot displaying the trajectories of the eigenvalues between the three control strategies. The cluster of eigenvalues to the left of the graph, with real part ≈ -2.53, are those related to the local area mode. These are unchanged between the three synthetic inertia control strategies showing that the DFIG has no effect on local mode participation. The remaining eigenvalues belong to the inter-area mode. As the control strategies are introduced, the eigenvalues shift further to the right hand side representing a decreased stability characterised by a reduction in damping ratio. These are given in Table 2 which shows how damping is reduced with the introduction of synthetic inertia. The damping ratio is reduced from 0.152 in the no control run, to 0.151 and then 0.130 in the one-loop and two-loop runs respectively. Similarly, the real component of the eigenvalue decreases from -2.335, to -2.298 then -2.023. The results suggest that the more effective the synthetic inertia control becomes, the lower the damping ratio for inter-area oscillations.

Table 2. Eigenproperties of dominant eigenvalues. Scenario 1—Base Case.

	No Control	**One-Loop**	**Two-Loop**
Damping Ratio	ζ	ζ	ζ
Local-area	0.143	0.143	0.143
Inter-area	0.152	0.151	0.130
Real Component	σ	σ	σ
Local-area	-2.524	-2.524	-2.524
Inter-area	-2.315	-2.298	-2.023

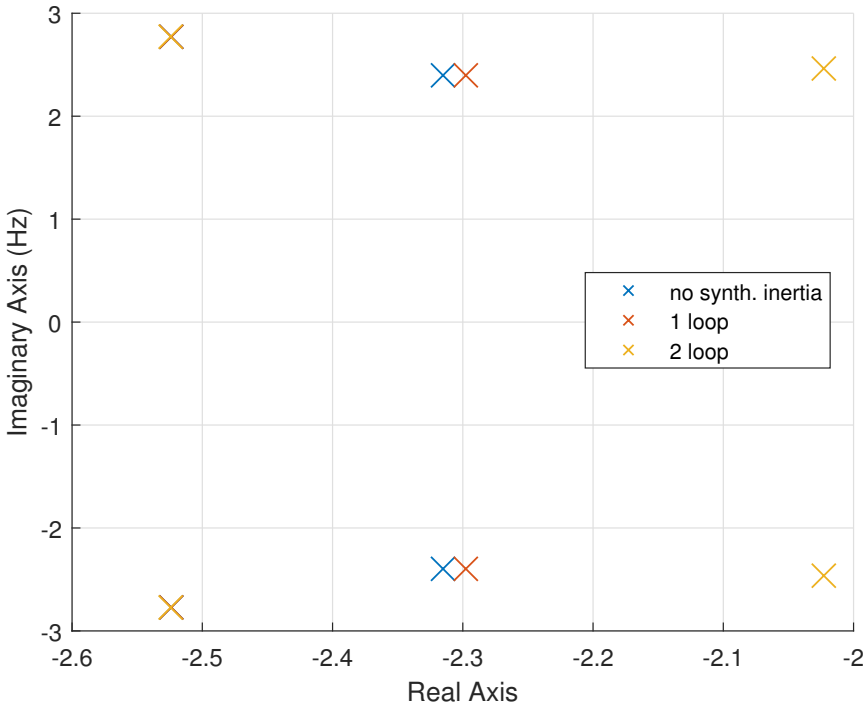

Figure 5. Pole-plot of dominant eigenvalues for $\Delta\omega$ modes—scenario 1. The cluster to the left shows the local-area mode which remains unchanged by different control strategies.

3.2. Scenario 2—Heavy Load

As described in the previous section, scenario 2 investigates the effect of different synthetic inertia schemes on a heavily loaded network. In this simulation, the balancing mechanism is removed from generator 1 such that the governor can no longer command the release of extra power in the event of a disturbance. When one of the other generators is taken offline, as in this simulation, the frequency does not recover and instead reduces to a new equilibrium.

The effects of synthetic inertia control on the electromechanical oscillations of the system are very similar to those in the base case of scenario 1. Once again, the local-area modes are unaffected and have therefore been omitted from any further analysis. The same pattern of reduced damping of the inter-area mode can be seen in Table 3. As the control strategies become more sophisticated, the system becomes less stable. The pole-plot in Figure 6 visualises the trend in Table 3 and shows a clear shift to the right.

Table 3. Scenario 2—Heavy Load.

	No Control	**One-Loop**	**Two-Loop**
Damping Ratio	ζ	ζ	ζ
Local-area	0.143	0.143	0.143
Inter-area	0.153	0.152	0.131
Real Component	σ	σ	σ
Local−area	−2.522	−2.522	−2.522
Inter−area	−2.329	−2.311	−2.034

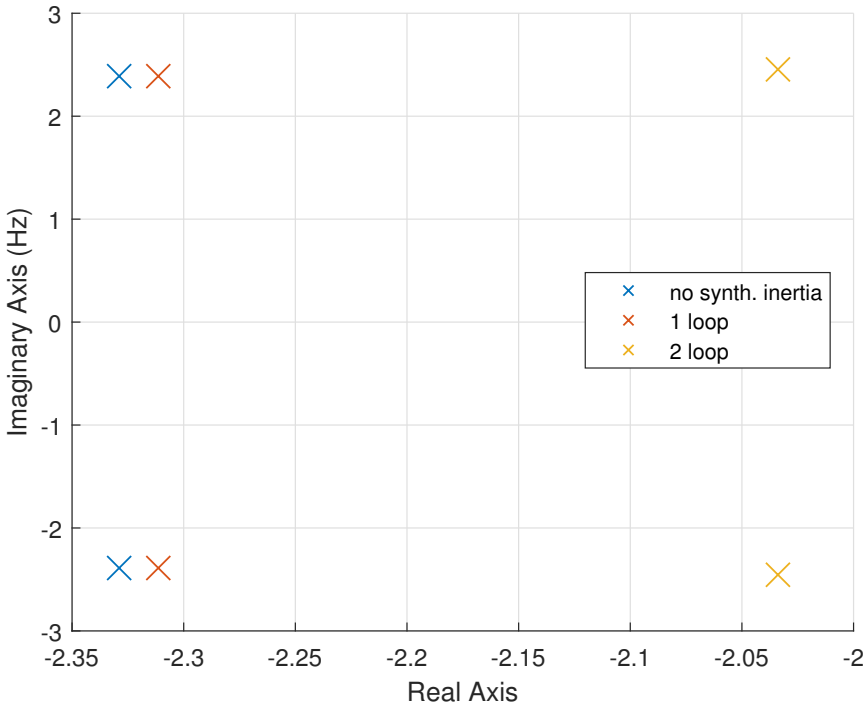

Figure 6. Pole-plot of dominant eigenvalues for $\Delta\omega$ modes—scenario 2.

3.3. Scenario 3—Weak Grid

The final scenario investigates the effect of a weak grid on the system eigenvalues. Governor action is restored to generator 1 but the tie-line connecting generator 1 to the rest of the network is reduced in strength. This is achieved by increasing the value of the impedance to simulate a longer transmission line. Such lines are common when a distant generating station must be connected to a load centre over a considerable distance. The impedance between the bus at generator 1 and the central has been increased from the initial value of $Z_{G1_{old}} = 0.002 + j0.2$ to $Z_{G1_{new}} = 0.006 + j0.6$, representing a three-fold increase in impedance.

The effect on the system eigenvalues can be seen in Figure 7. Unsurprisingly, the system begins much less damped than the base case of scenario 1. The eigenvalues find themselves further to the right hand side towards increasing instability due to the weak grid criterion which has reduced the overall damping of all oscillations. As the control strategies are applied, the same pattern of reduced damping ratios can be seen to recur. Table 4 shows that the damping ratio of the inter-area mode is reduced from 0.133 to 0.131 then to 0.102 for the no-control, 1-loop and 2-loop systems respectively.

Table 4. Scenario 3—Weak Grid.

	No Control	**One-Loop**	**Two-Loop**
Damping Ratio	ζ	ζ	ζ
Local-area	0.141	0.141	0.141
Inter-area	0.133	0.131	0.102
Real Component	σ	σ	σ
Local−area	−2.637	−2.638	−2.638
Inter−area	−1.897	−1.872	−1.509

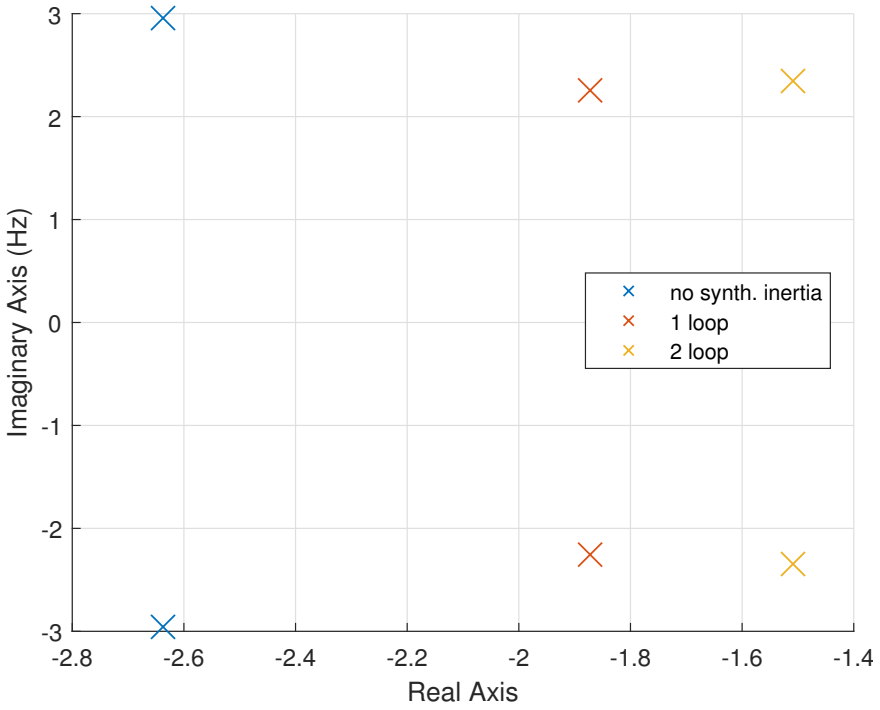

Figure 7. Pole-plot of dominant eigenvalues for $\Delta\omega$ modes—scenario 3.

4. Conclusions

This work has explored the effects of two different methods of synthetic inertia provision on small-signal stability in the context of a power system. A three-generator model with an added wind-farm was developed for the sole purpose of linearisation and small-signal analysis was conducted to explore the eigenproperties of different controller topologies and their effects on the electromechanical oscillations between generators. Three network scenarios were identified and tested, these being: base case; heavily loaded system, and a weaker grid.

The results show a trend of decreasing small-signal stability as synthetic inertia is introduced, with the more sophisticated two-loop synthetic inertia controller showing the greatest reduction. These results are shown in Figures 5–7 and Tables 2–4, where the trajectories of the eigenvalues demonstrate a decreasing damping ratio and a less-negative real part. The base case, heavy load and weak grid simulations all mirror this effect. This suggests that the more a DFIG tries to emulate the action of a synchronous generator, the more it participates in inter-area oscillations. Overall, this has been characterised by a reduction in system damping ratio relating to those eigenvalues dominant to the shared mechanical modes of the synchronous generators.

This study has focused on modelling and simulation, yet the real-world applications of this study may present themselves in future electrical networks between the participation of wind farms in synthetic inertia provision. There may exist a trade-off between the degree of participation in frequency response and the greater instability associated with electromechanical oscillations. As the penetration of low-inertial renewable energy systems increases, it is likely that the phenomena of coupled oscillatory modes will become more apparent.

Author Contributions: Conceptualisation, O.A.-L; methodology, E.L.; software, E.L.; validation, E.L., O.A.-L. and D.C.-G.; formal analysis, E.L.; investigation, E.L.; resources, O.A.-L. and D.C.-G; data curation, E.L.; writing–original draft preparation, E.L.; writing–review and editing, E.L., O.A.-L. and D.C.-G.; visualisation, E.L.; supervision, O.A.-L. and D.C.-G.; project administration, E.L.

Funding: This work has been funded by the EPSRC, project reference number EP/L016680/1.

Conflicts of Interest: The authors declare no conflict of interest.

Nomenclature

ω_e	Grid angular frequency
ω_r	DFIG rotor speed
f	System frequency
P_{mpp}	Power from maximum power tracker
P_{in}	Power from inertia controller
P_{ref}	Reference power sent to converter
K_1,K_2	Synthetic inertia gains
K_{iP}	Power controller gain
λ_{ds},λ_{qs},λ_{dr},λ_{qr},	Two-axis DFIG stator and rotor fluxes
K,T_1,T_2,T_3	Governor gain and time constants
v_{ds},v_{qs},v_{dr},v_{qr}	Two-axis stator and rotor voltage components
R_s,R_r	stator and rotor resistance
L_{ls},L_{lr},L_m	DFIG stator, rotor and mutual inductance
T_{em},T_{mech},T_{damp}	Electrical, mechanical and damping torque
J	DFIG inertia constant
p	DFIG pole pairs
X_d,X_q	Two axis synchronous reactance
$X_d^{'}$,$X_q^{'}$	Two axis transient reactance
$T_{d0}^{'}$,$T_{q0}^{'}$	Two axis transient time constant
H	Inertia constant
D	Damping constant

Appendix A

This section contains the equations used for modelling the various network elements as well as the simulation parameters as shown in Tables A1 and A2.

The synchronous machines are modelled according to the dq-transient model in [11]. The following equations give the 4th order system.

$$v_{qs} = E_q^{'} - R_s i_q - X_d i_d \tag{A1}$$

$$v_{ds} = E_d^{'} - R_s i_d - X_q i_q \tag{A2}$$

$$E_q^{'} = \frac{1}{T_{d0}^{'}} \int [E_f - E_q^{'} - i_d(X_d - X_d^{'})]\, dt \tag{A3}$$

$$E_d^{'} = \frac{1}{T_{q0}^{'}} \int [E_f - E_d^{'} - i_q(X_q - X_q^{'})]\, dt \tag{A4}$$

$$T_{em} = -(E_q^{'} i_q + E_d^{'} i_d) \tag{A5}$$

$$slip = \frac{1}{2H} \int (T_{em} + T_{mech} - T_{damp})\, dt \tag{A6}$$

$$\delta_e = \int (\omega_r - \omega_e)\, dt \tag{A7}$$

The governor model is taken from the IEEE Governor Standards in [18] titled 'type-2 speed governing model' with gains and time constants given in Table A1.

The DFIG is modelled as a 5th order system in the dq-reference frame according to [11] where the fluxes are chosen as the state variables.

$$\lambda_{qs} = \int v_{qs} - w_e\lambda_{ds} - \frac{R_s}{L_{ls}}(\lambda_{qs} - \lambda_{mq})\,dt \tag{A8}$$

$$\lambda_{ds} = \int v_{ds} + w_e\lambda_{qs} - \frac{R_s}{L_{ls}}(\lambda_{ds} - \lambda_{md})\,dt \tag{A9}$$

$$\lambda_{qr} = \int v_{qr} - (w_e - \omega_r)\lambda_{dr} - \frac{R_r}{L_{lr}}(\lambda_{qr} - \lambda_{mq})\,dt \tag{A10}$$

$$\lambda_{dr} = \int v_{dr} + (w_e - \omega_r)\lambda_{qr} - \frac{R_r}{L_{lr}}(\lambda_{dr} - \lambda_{md})\,dt \tag{A11}$$

$$\lambda_{md} = L_M\left(\frac{\lambda_{ds}}{L_{ls}} - \frac{\lambda_{dr}}{L_{lr}}\right) \tag{A12}$$

$$\lambda_{mq} = L_M\left(\frac{\lambda_{dq}}{L_{ls}} - \frac{\lambda_{dq}}{L_{lr}}\right) \tag{A13}$$

$$T_{em} = \frac{3p}{2}(\lambda_{qr}i_{dr} - \lambda_{dr}i_{qr}) \tag{A14}$$

$$\omega_r = \frac{p}{J}\int (T_{em} - T_{mech} - T_{damp})\,dt \tag{A15}$$

Table A1. Synchronous Machine Model Parameters.

Variable	Gen 1	Gen 2	Gen 3
Rated Power (MW)	1000	200	200
Rated Voltage (kV)	18	18	18
R_s (pu)	0.0048	0.001	0.001
X_q (pu)	1.66	1.96	1.96
$X_q^{'}$ (pu)	0.57	0.262	0.262
X_d (pu)	1.79	2.04	2.04
$X_d^{'}$ (pu)	0.335	0.266	0.266
$T_{q0}^{'}$ (s)	0.41	0.9	0.9
$T_{d0}^{'}$ (s)	7.9	6.0	6.0
H (s)	3.77	2.7	2.7
D (pu)	2.0	2.0	2.0
Gov. K	50.0	-	-
Gov. T1 (s)	0.1	-	-
Gov. T2 (s)	0.1	-	-
Gov. T3 (s)	0.04	-	-
Gov. T4 (s)	0.04	-	-

Table A2. DFIG model parameters.

Rated Power (MW)	100	L_{lr} (pu)	0.0996
Rated Voltage (kV)	18	L_m (pu)	3.935
R_s (pu)	0.0049	J (kg m^2)	2.84×10^5
R_r (pu)	0.0055	D (pu)	0.01
L_{ls} (pu)	0.0924	p	2

References

1. Ekanayake, J.B.; Holdsworth, L.; Wu, X.G.; Jenkins, N. Dynamic Modeling of Doubly Fed Induction Generator Wind Turbines. *IEEE Trans. Power Syst.* **2003**, *18*, 803–809. [CrossRef]
2. Edrah, M.; Lo, K.L.; Anaya-Lara, O. Impacts of High Penetration of DFIG Wind Turbines on Rotor Angle Stability of Power Systems. *IEEE Trans. Sustain. Energy* **2015**, *6*, 759–766. [CrossRef]
3. Roberts, C. *Review of International Grid Codes*; U.S. Department of Energy, Grid Modernization Lab Consortium: Washington, DC, USA, 2018.
4. Xia, Y.; Yuan, R.; Zhang, Z.; Hu, W. Damping Inter-area Modes of Oscillation and Improving Transmission Capacity Using Global PSS. In Proceedings of the 2009 International Conference on Energy and Environment Technology, Guilin, China, 16–18 October 2009.
5. Hydro-Québec TransEnergie. Transmission Provider Technical Requirements for the Connection of Power Plants to the Hydro-Québec Transmission System. Available online: http://www.hydroquebec.com/transenergie/fr/commerce/pdf/2_Requirements_generating_stations_D-2018-145_2018-11-15.pdf (accessed on 5 September 2019).
6. White, S. National Grid. Grid Code Frequency Response Working Group—Synthetic Inertia. Available online: https://www.nationalgrideso.com/document/10331/download (accessed on 5 September 2019).
7. Ackermann, T. *Technical Regulations for the Interconnection of Wind Farms to the Power Systems*; John Wiley & Sons Ltd.: Hoboken, NJ, USA, 2005; Chapter 7.
8. Dreidy, M.; Mokhlis, H.; Mekhilef, S. Inertia response and frequency control techniques for renewable energy sources: A review. *Renew. Sustain. Energy Rev.* **2017**, *69*, 144–155. [CrossRef]
9. Sun, Y.; Zhang, Z.; Li, G.; Lin, J. Review on frequency control of power systems with wind power penetration. In Proceedings of the 2010 International Conference on Power System Technology, Hangzhou, China, 24–28 October 2010.
10. Zhang, Z.; Wang, Y.; Li, H.; Su, X. Comparison of inertia control methods for DFIG-based wind turbines. In Proceedings of the 2013 IEEE ECCE Asia Downunder, Melbourne, VIC, Australia, 3–6 June 2013.
11. Ong, C.M. *Dynamic Simulation of Electrical Machinery*; McGraw-Hill: New York, NY, USA, 1997; Chapter 6.
12. Campos-Gaona, D.; Moreno-Goytia, E.L.; Anaya-Lara, O. Fault Ride-Through Improvement of DFIG-WT by Integrating a Two-Degrees-of-Freedom Internal Model Control. *IEEE Trans. Ind. Electron.* **2013**, *60*, 1133–1145. [CrossRef]
13. Kundur, P. *Power System Stability and Control*; McGraw-Hill: New York, NY, USA, 1994; Chapter 12.
14. Ma, J.; Qiu, Y.; Li, Y.; Zhang, W.; Song, Z.; Thorp, J. Research on the Impact of DFIG Virtual Inertia Control on Power System Small-Signal Stability Considering the Phase-Locked Loop. *IEEE Trans. Power Syst.* **2017**, *32*, 2094–2105. [CrossRef]
15. Quintero, J.; Vittal, V.; Heydt, G.T.; Zhang, H. The Impact of Increased Penetration of Converter Control-Based Generators on Power System Modes of Oscillation. *IEEE Trans. Power Syst.* **2014**, *29*, 2248–2256. [CrossRef]
16. Jiaying, S.; Chen, S. Impact of DFIG wind power on power system small signal stability. In Proceedings of the 2013 IEEE PES Innovative Smart Grid Technologies Conference (ISGT), Washington, DC, USA, 24–27 February 2013.

17. Wang, Z.; Shen, C.; Liu, F. Impact of DFIG with phase lock loop dynamics on power systems small signal stability. In Proceedings of the 2014 IEEE PES General Meeting Conference and Exposition, National Harbor, MD, USA, 27–31 July 2014.
18. NEPLAN, IEEE Standards. Turbine-Governor Models. Available online: https://www.neplan.ch/wp-content/uploads/2015/08/Nep_TURBINES_GOV.pdf (accessed on 5 September 2019).